Available online at www.sciencedirect.com
ScienceDirect
Journal of the European Ceramic Society 27 (2007) 1991–1998
www.elsevier.com/locate/jeurceramsoc

Comparison of two different precipitation routes leading to Yb doped Y_2O_3 nano-particles

Johanne Mouzon *, Patricia Nordell, Adrien Thomas, Magnus Odén

Division of Engineering Materials, Luleå University of Technology, SE-971 87 LULEÅ, Sweden

Received 27 January 2006; received in revised form 29 May 2006; accepted 31 May 2006
Available online 28 July 2006

Abstract

Two different precipitation routes leading to $(Yb_xY_{1-x})_2O_3$ nano-particles (with $x=0$; 0.027; and 0.31) were compared, namely, precipitation of hydroxynitrate platelets and amorphous carbonate spherical particles. For both methods, the particle morphology was observed by scanning electron microscopy. X-ray diffraction studies of the unit cell, energy dispersive X-ray analysis and inductive coupled plasma spectroscopy were used to check the ytterbium distribution. The precipitation of amorphous carbonate was found to produce particles with uniform morphology and homogeneous distribution of ytterbium, while hydroxide precipitation favours the formation of hard and dense ytterbium-rich agglomerates. These differences are discussed in terms of precipitation, growth and agglomeration behaviour. The sinterability of both resulting powders is also discussed.

Keywords: Powders-chemical preparation; Doping; Defects; Sintering; Y_2O_3

1. Introduction

Ytterbium doped yttria ($Yb:Y_2O_3$) is a promising laser material. Y_2O_3 has a thermal conductivity twice as large as that of YAG[1] and Yb^{3+} is a very attractive dopant for efficient diode-pumped solid-state lasers. Yb^{3+} shows high quantum efficiency, weak non-radiative transitions, large crystal-field splitting, millisecond-lifetime of the metastable $^2F_{5/2}$ state, and intense inter-Stark $^2F_{5/2} \leftrightarrow {}^2F_{7/2}$ transitions.[2] However, $Yb:Y_2O_3$ single crystals are very difficult to grow. Recently, it has been shown that polycrystalline Nd:YAG ceramic lasers could be fabricated with properties equalling those of Nd:YAG single-crystal.[3] Based on these observations, polycrystalline $Yb:Y_2O_3$ ceramic appears to be a potential candidate for laser applications.

In order to manufacture a transparent polycrystalline ceramic by sintering for laser application, the starting powder must meet several requirements. On one hand, a small particle size is necessary to enhance sintering activity, since the driving force for sintering can be considered to be, as a first approximation, the reduction of the surface area of the porous compact. This will speed up material transport and enable the sintering to reach full density more rapidly and far below the melting temperature of the crystal. On the other hand, low agglomeration is desirable to avoid density gradient that are responsible for differential sintering, i.e. agglomerates with low-pore coordination numbers shrink first and locally causing porous regions with high coordination number to develop between agglomerates. These highly coordinated regions are then kinetically unlikely to disappear, unless particle rearrangement occurs.[4] Any remaining porosity is unacceptable for optical applications, since it will cause light scattering. Therefore, agglomeration in the starting powder must be limited.

Purity is also an important issue to be controlled, both for the sintering process and for the future laser material. For instance, it is well-known that only a few hundreds parts per million of MgO is responsible for alumina to sinter to full density and transparency.[5] Thus, high purity of the raw materials is required in order to be able to sinter in a controlled way, with or without addition of sintering aids. From the laser point of view, impurities are often responsible for energy transfers and modification of the average crystal field strength.[6] Impurities can also modify the point defect distribution of the ionic crystal leading to discoloration. All these phenomena are detrimental to the laser properties.

* Corresponding author.
E-mail address: johmou@ltu.se (J. Mouzon).

0955-2219/$ – see front matter © 2006 Elsevier Ltd. All rights reserved.
doi:10.1016/j.jeurceramsoc.2006.05.103

Another requirement is that dopant has to be as well distributed as possible in the host-matrix. Although the simple energy state of Yb^{3+} prevent self-quenching, it is better to avoid clustering and promote random distribution to obtain homogenous bulk properties. Regarding ceramic processing, it is often better to start with a powder with a distribution of doping elements similar to the desired distribution in the final material. Doping by addition of foreign particles containing the dopant and subsequent solid-state interdiffusion under heating will inevitably influence sintering if performed simultaneously. If doping is performed in a thermal pre-treatment, grain growth is usually required to achieve good mixing, which reduces the sinterability of the powder. Therefore, in order to be able to control sintering, it is preferable to begin with a non-agglomerated powder, in which the dopant is homogeneously distributed directly during powder synthesis. Co-precipitation appears as a candidate to fulfil all these criteria.

Recently, two new precipitation methods have been developed leading to nano-sized particles of yttria with a limited amount of agglomeration. The first method consists in synthesising open networks of platelets,[7] nano-rods,[8] or foams[9] that decompose upon heating into spherical nano-particles. This method presents two advantages. It avoids agglomeration of the final powder, since the original morphology of the precursor is not retained after calcination. In addition, since the two former methods involve crystallisation of the precursor, impurities are left or rejected in the solution, thereby improving the purity of the powder.

The second approach involves the synthesis of carbonate nano-particles. Carbonate precursor are considered to be less sensitive to the formation of hard agglomerates during dewatering, because they do not form hydrogen bonds with water.[10] This method has been shown to be very successful to co-precipitate yttrium and aluminium,[11,12] especially when an amorphous precursor was obtained. Specifically, it resulted in better cation homogeneity.

In this paper, we investigate the ability of both methods to synthesise $Yb:Y_2O_3$ nano-particles in terms of dopant distribution and purity.

Table 1
Description of the different samples

Sample	Synthesis	Yb (at%)
0Yb:OH	Yttrium hydroxynitrate platelets	0
2.7Yb:OH	Yttrium hydroxynitrate platelets	2.7
31Yb:OH	Yttrium hydroxynitrate platelets	31
0Yb:CO	Amorphous yttrium carbonate	0
2.7Yb:CO	Amorphous yttrium carbonate	2.7
31Yb:CO	Amorphous yttrium carbonate	31
0Yb:HOX	0Yb:OH calcined at 1100 °C/4 h	0
2.7Yb:HOX	2.7Yb:OH calcined at 1100 °C/4 h	2.7
31Yb:HOX	31Yb:OH calcined at 1100 °C/4 h	31
0Yb:COX	0Yb:CO calcined at 1100 °C/4 h	0
2.7Yb:COX	2.7Yb:CO calcined at 1100 °C/4 h	2.7
31Yb:COX	31Yb:CO calcined at 1100 °C/4 h	31

2. Experimental

A precursor of each concept was chosen in literature and their synthesis were repeated, namely: yttrium hydroxynitrate platelets with transient morphology[7] and spherical amorphous particles of yttrium carbonate precursor.[8] For the sake of clarity, flow charts presenting both procedures are shown in Fig. 1. Both methods were carried out without ytterbium and by substituting 2.7 and 31 at% of the nominal yttrium concentration by ytterbium (see Table 1 for details of the different samples).

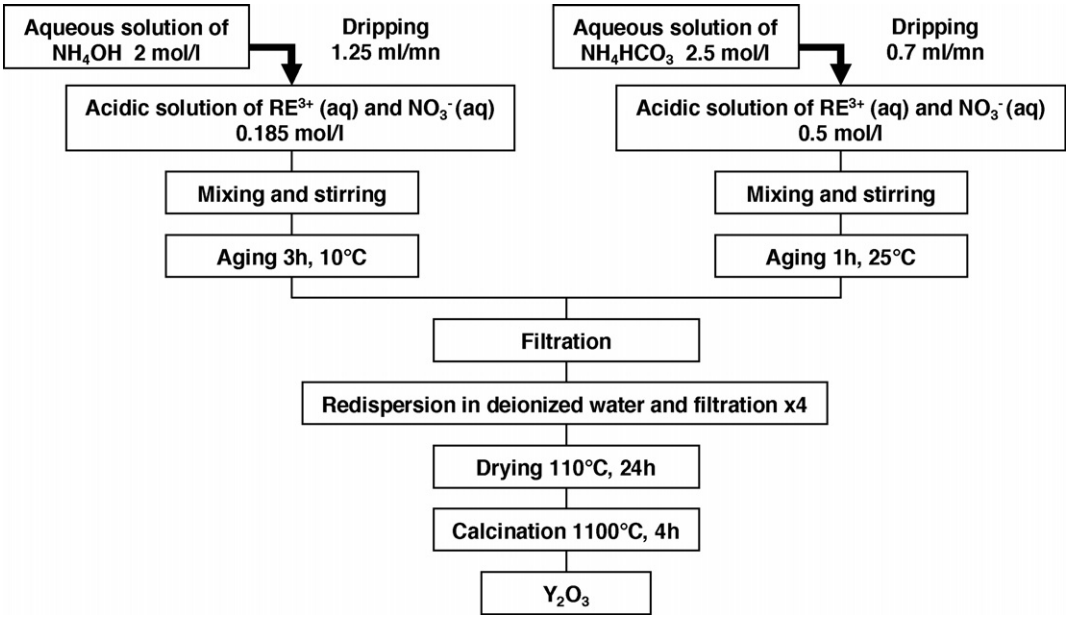

Fig. 1. Flow chart of two different routes leading to nano-particles of Y_2O_3.

2.1. Hydroxynitrate route

A 0.185 mol/l mother solution of yttrium nitrate (99.99% Rhodia) was prepared by dissolution with ion-exchanged water (resistivity >6 MΩ cm). When doping was performed, 2.7 and 31 at% of yttrium was substituted by ytterbium (ytterbium nitrate pentahydrate, 99.9% Aldrich). A 2 mol/l ammonia water solution (Suprapur®, Merck) was used as a precipitant. A 50 ml of the precipitant was dripped at a rate of 1.25 ml/min into 100 ml of the mother solution, which was held at a temperature of 10 °C. The precipitate was then left to age for 3 h at the same temperature and then recovered by suction filtration. In order to reduce by-products of the reaction to a minimum level in the precipitate, dispersion in ion-exchanged water and filtration were repeated four times.

2.2. Normal carbonate route

A 0.37 mol/l mother solution of yttrium nitrate and a 2.5 mol/l ammonium hydrogen carbonate (AHC) solution (99.5%, Fluka) used as precipitant were prepared by dissolution. Similar to the hydroxynitrate route, 2.7 and 31 at% ytterbium was also substituted to yttrium nitrate for doping. 28 ml of the precipitant was dripped at a rate of 0.7 ml/min into 70 ml of the mother solution, which was held at a temperature of 25 °C. The precipitate was then left to age for 1 h. It was recovered and washed in the same manner as the hydroxynitrate precursor.

2.3. Drying, calcination and sintering

During filtration all precursors formed cakes which were dried at 110 °C in an oven equipped with a fan to enhance mass transport. Drying was considered to be ended when no more weight loss could be observed. Calcination was performed at 1100 °C in a flowing oxygen atmosphere. A heating rate of 300 °C/h and a dwell period of 4 h were used. The calcined yttria powders doped with 31 at% ytterbium were sintered in order to homogenise the distribution of ytterbium by increasing diffusion and grain growth at high temperatures. Pellets were uniaxially pressed in a 14-mm-diameter die under 10 MPa. This was followed by cold isostatic pressing under 200 MPa pressure. The resulting pellets were sintered at 1600 °C for 7 h in air.

2.4. Characterisation

Particle morphology was observed by scanning electron microscopy (SEM, JSM 6460lv, JEOL, Japan). A small quantity of powder was dispersed by ultrasonication in methanol and one drop was deposited on an aluminium substrate. Samples were coated by a thin layer of gold to minimise charging.

Distribution of the dopant was checked by using back-scattered electron imaging and energy-dispersive X-ray analysis (Oxford Instruments, United Kingdom). In order to obtain a flat surface, powder was mixed with epoxy resin and hardener, and then cast into a cylindrical mould. After hardening, the mounted sample was polished using diamonds with an averaged grain size of 1/4 μm in the final step.

X-ray diffractometry (XRD) with a Philips X'pert system equipped with a secondary monochromater and Cu Kα radiation was used for phase identification and lattice parameter determination. Silicon powder (99% purity) was mixed with the calcinated powders and used as calibrant in order to obtain quantitative lattice parameter information. The sintered powders were pulverised using agate mortar in order to release residual stresses that might have affected the measurements. Commercial powders of pure yttrium and ytterbium oxides (99.99% REacton, Alfa Aesar) were also used as reference samples. Peak positions were determined by least square fitting Gaussian functions to the 222 and 400 diffraction lines of yttria. The same procedure was used to check if Y and Yb had formed solid solutions in the case of the platelet-like precursors. In this case, a zirconium powder (98% purity) was used as calibrant to determine the peak locations.

Chemical analysis to assess doping content and purity level was performed using both ICP-AES and HR-ICP-MS. Trace elements were analysed by 50 scans over the whole mass region, which corresponds to a total measuring time of 300 s.

3. Results and discussion

Fig. 2 shows the powder morphology both before and after calcination of the two different precursors, namely, the hydroxide and carbonate powders. No obvious difference between the undoped and heavily doped precursors could be distinguished for both methods. In the case of the precipitation by ammonia water, platelets can be observed (Fig. 2(a)). During calcination, the platelets decompose into small rounded particles more or less bonded to one another as can be seen in Fig. 2(c). On the other hand, the carbonate precursors precipitated by AHC are composed of spherical particles that formed during precipitation. Fig. 2(b and d) show that these particles remain even after calcination with some slight degree of bridging.

All precursors precipitated by ammonia water exhibit nearly identical diffractograms as the one depicted in Fig. 3(a). This diffractogram resembles those of $Y_2(OH)_{5.14}(NO_3)_{0.86}{\cdot}H_2O$ and $Y_2(OH)_5(NO_3).1.5H_2O$.[13] The platelets are of poor crystalline quality and it is the reason for the high background level. Values of the interplanar spacing from the peak located at around 28.6° for all hydroxide precursors are given in Table 2. The formation of a solid solution cannot be established by comparing the cases of 0 and 2.7 at% ytterbium doping. However, a doping of 31 at% ytterbium results in a relative linear shrinkage of 0.34% for the corresponding interplanar spacing indicating solid solution. The formation of a solid solution by substitution is not surprising, since both yttrium and ytterbium hydroxynitrates with close compositions of those precipitated in this work

Table 2
Interplanar distance calculated from the peak around 28.6° for both doped and undoped hydroxynitrate precursors

Yb_0 (at%)	0	2.7	31
d (Å)	3.1103 ± 0.0004	3.1104 ± 0.0003	3.0985 ± 0.0003

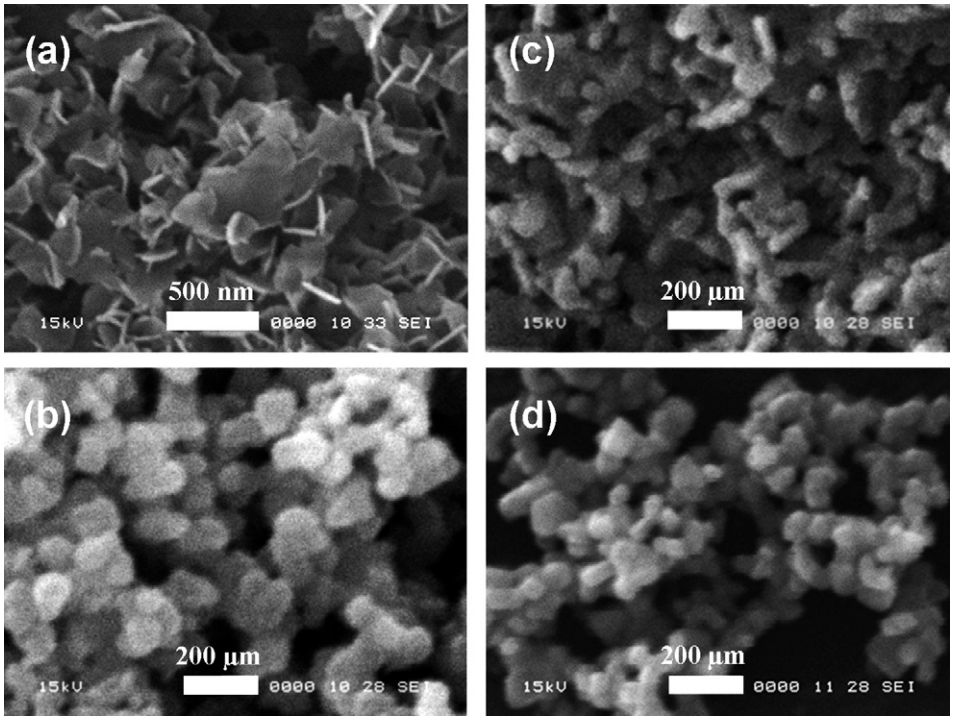

Fig. 2. Typical scanning electron micrographs of the precursors: (a) 0Yb:OH, (b) 31Yb:CO and the respective oxides: (c) 0Yb:HOX, (d) 31Yb:COX.

have been found to crystallise in orthorhombic structures under hydrothermal conditions.[14]

The diffractogram of the doped precursors precipitated by AHC is shown in Fig. 3(b). The high background level and the lack of diffraction lines indicate an amorphous structure. In the case of the undoped sample (not shown here), weak diffraction lines could be distinguished that are consistent with yttrium normal carbonate $Y_2(CO_3)_3{\cdot}2H_2O$.[15]

The X-ray diffractograms of all the calcinated powders (not shown here) are consistent with yttria,[16] although shifted towards higher 2θ values for the doped samples. Full solubility is expected for mixture of yttrium and ytterbium oxides, since both oxides crystallise in the bixbyite structure (space group $Ia(T_h^7)$ with $Z=16$) and yttrium and ytterbium have very close ionic radii (87 and 90 pm, respectively).

Table 3 presents the unit cell parameters of the different synthesised oxides, as well as for the Y_2O_3 and Yb_2O_3 reference samples. The unit cell parameters are also plotted in Fig. 4. The values found for the undoped samples are quite constant with an average value of 10.605 Å. This compares favourably with a value of 10.604 found in literature.[16] Table 3 contains also the apparent content of ytterbium, Yb_a, which was calculated based on the measured unit cell parameters and Panitz and Vegard's law.[17] Dimensions of 10.605 Å and 10.435 Å for the unit cells of yttrium and ytterbium oxides, respectively, were used for the calculations. The Yb_a values obtained for the carbonate-derived powders agree well with the nominal compositions, Yb_0. However, calculations of Yb_a for the hydroxynitrate-derived powders

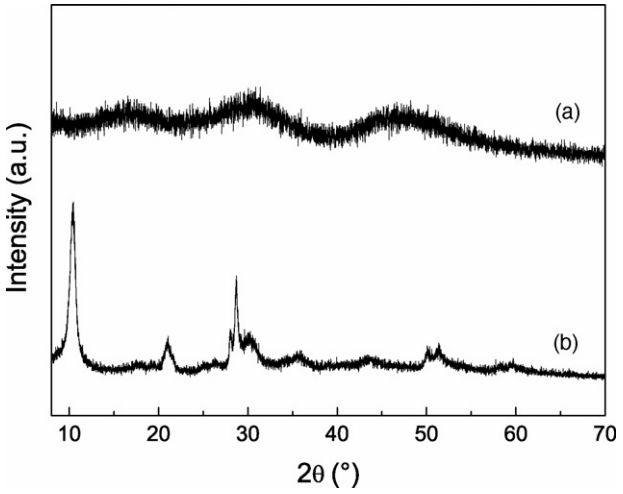

Fig. 3. X-ray diffractograms of: (a) 31Yb:OH; (b) 31Yb:CO.

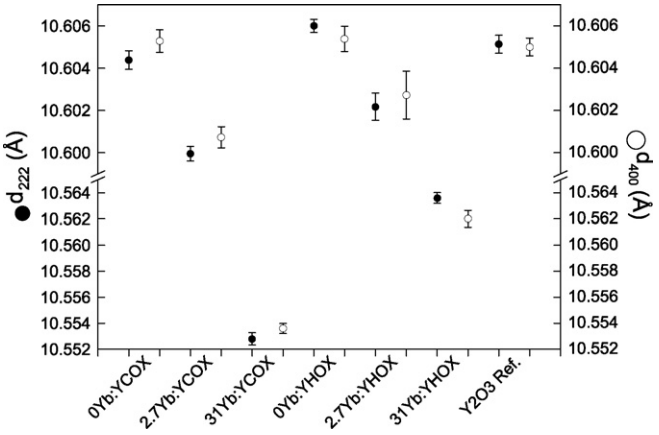

Fig. 4. Unit cell parameters of the different powders with error bars.

Table 3
Unit cell dimensions of the synthesized oxides according to X-ray powder diffraction

Yb_0 (at%)	Platelets with transient morphology synthesis				Amorphous carbonate synthesis				Y_2O_3 Ref. sample		Yb_2O_3 Ref. sample	
	a_{222} (Å)	a_{400} (Å)	Yb_a (at%)	Yb_{ICP} (at%)	a_{222} (Å)	a_{400} (Å)	Yb_a (at%)	Yb_{ICP} (at%)	a_{222} (Å)	a_{400} (Å)	a_{222} (Å)	a_{400} (Å)
0	10.606	10.605			10.604	10.605			10.605	10.605	10.435	10.436
2.7	10.602	10.603	1.5	2.8	10.600	10.601	2.8	2.7				
31	10.564	10.562	24.9		10.553	10.554	30.5					
31[a]	10.560	10.562	26.1		10.552	10.554	30.8					

Nominal composition (Yb_0) is compared with ytterbium apparent content (Yb_a) and ICP-MS elemental analysis (Yb_{ICP}).
[a] Sintered at 1600 °C for 7 h, then pulverised.

show lower values than the nominal compositions. The nominal compositions of 2.7Yb:COX and 2.7Yb:HOX were confirmed by ICP measurements (Yb_{ICP}, Table 3). Thus, no ytterbium was lost during synthesis and ytterbium loss cannot be responsible for the larger unit cell parameter found for 2.7Yb:HOX and 31Yb:HOX in comparison with those found for 2.7Yb:COX and 31Yb:COX.

Fig. 5 shows two scanning electron micrographs of the 31Yb:OH and 31Yb:CO precursors. In Fig. 5(a), in addition to the dark agglomerates of platelets that represents most of the powder, bright chip-like particles can be observed, thereby indicating the presence of a second phase. The size of these chip-like particles ranges from 2 to 200 μm in length. Bright chip-like particles can also be observed in the powder after calcination (not shown here) and contain only yttrium and ytterbium apart from oxygen. Higher ytterbium content was found by EDX analysis in the bright regions in comparison with the dark regions, as shown in Table 4. Since ytterbium has an atomic number almost twice as large as yttrium it will give rise to Z-contrast in the micrographs and the brighter areas will contain a higher ytterbium content than the nominal composition and vice versa for the darker regions. The X-ray diffractograms from this microstructure will give rise to convoluted peaks containing information from both types of regions. This explains the lower theoretical ytterbium contents found in Table 3 for the 2.7Yb:HOX and 31Yb:HOX samples, since they were inferred from the peak locations. On the other hand, the appearance of the 31Yb:CO sample by backscattered electron imaging is homogenous, as it can be seen in Fig. 5(b). Constant ytterbium content close to the nominal composition was found by EDX analysis both in the as-synthesised and calcinated powders (31Yb:CO and 31Yb:COX in Table 4). This indicates an excellent mixing of both rare-earth cations directly in the precipitated particles.

All observed bright chip-like particles appear to be dense and to be covered by platelets on one side and by more equiaxed but irregular particles on the other side (Fig. 6(a)), these latter being richer in ytterbium than the former as they appear brighter in Fig. 6(b). The layer of platelets seems to be tightly bonded to the chip-like particle and was found to extend from a single layer up to 100 μm. Fig. 6(c) shows a crack in a bright chip-like particle revealing that it consists of equiaxed grains with sizes around 300 nm and below, as indicated by the arrows.

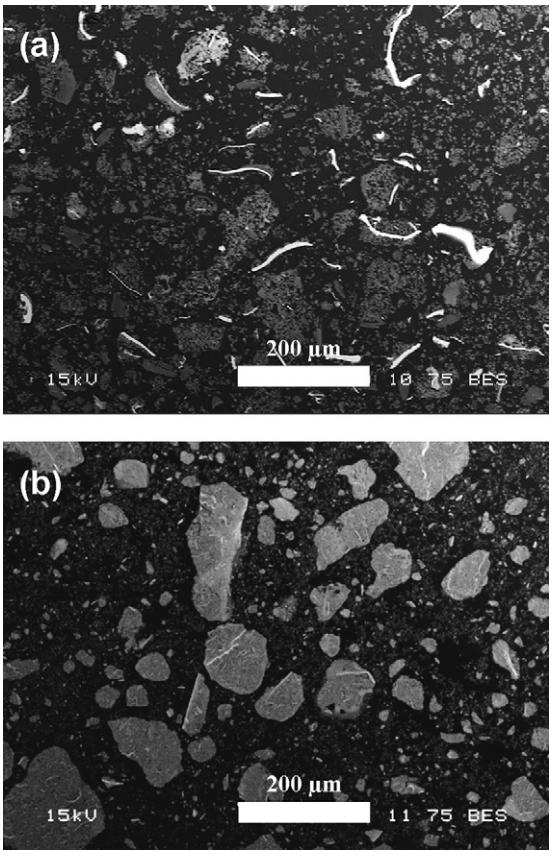

Fig. 5. Scanning electron micrographs recorded in backscattered electron mode of powder particles embedded in epoxy resin: (a) 31Yb:OH and (b) 31Yb:CO.

Table 4
Ytterbium content determined by EDX spot analysis in dark and bright regions for all samples initially doped with 31 at%

Sample	31Yb:OH	31Yb:HOX	31Yb:CO	31Yb:COX
Yb_{dark} (at%)	19.7 ± 3.1 (9)	19.8 ± 5.6 (27)	30.2 ± 4.3 (34)	30.1 ± 2.0 (30)
Yb_{bright} (at%)	51.6 ± 8.4 (13)	55.5 ± 4.3 (9)		

In brackets, number of analysed spots.

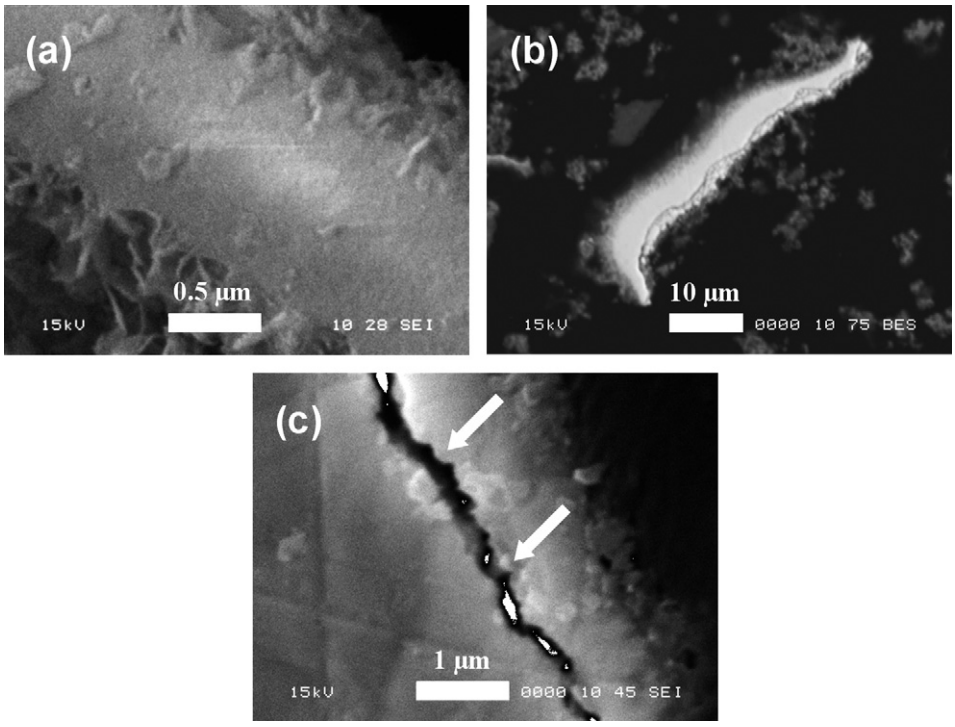

Fig. 6. Scanning electron micrographs showing: (a) the structure on both sides of a bright chip-like particle in 31Yb:OH (secondary electrons), (b) a bright chip-like particle in 31Yb:HOX (backscattered electrons), and (c) a crack in another bright chip-like particle in 31Yb:OH (secondary electrons).

In order to homogenise the distribution of ytterbium, pellets of the 31Yb:COX and 31Yb:HOX powders were pressed and sintered at 1600 °C for 7 h. In the case of 31Yb:HOX, Fig. 7(a) shows that bright regions of different sizes are still present after long heat treatment at high temperature. After sintering, Yb_a increases from 24.9 to 26.1 at% (Table 3). However, this is still below the expected value when ytterbium is homogeneously dispersed, i.e. nominal composition. Very long thermal treatments would be required to distribute ytterbium throughout the sample.

Moreover, numerous flaws as the ones shown in Fig. 7(b) can be observed in the sintered 31Yb:HOX sample. These flaws appear to be elongated and probably formed alongside chip-like particles. Since they are dense and hard, the chip-like particles prevent achieving homogeneous compaction densities around them. Low-density regions therefore undergo high shrinkage and development of porosity during sintering. The fact that porosity constantly develops only on one side of the chip-like particles is consistent with the asymmetric layers on each side. The layer of platelets observed to form on one side is already bonded to the chip-like particle before compaction. Thus, it should give rise to a high density during pressing in comparison with the opposite side.

On the other hand, sintering of the 31Yb:COX powder produces a final sample with homogeneous distribution of ytterbium, as indicating by the Yb_a value close to nominal composition in Table 3. Furthermore, fewer and smaller flaws developed in the material, thereby resulting in higher densities. This is certainly due to fewer hard agglomerates in the powder.

How the chip-like particles formed is unclear and requires further investigation. Nevertheless, the chip-like particles consist of

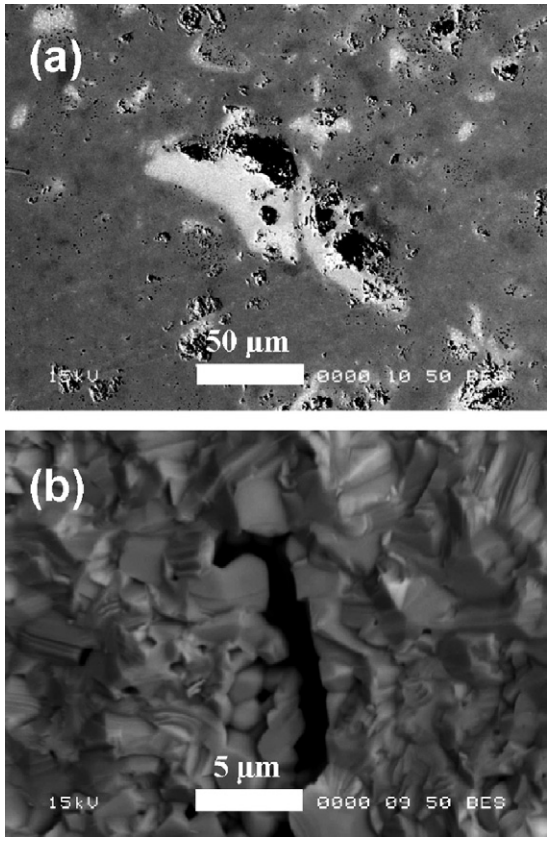

Fig. 7. Scanning electron micrographs showing: (a) the presence of ytterbium-rich regions on the polished surface of the 31Yb:HOX sample sintered at 1600 °C for 7 h, (b) a typical flaw induced by an ytterbium-rich aggregate and observed in the same sample on a fracture surface.

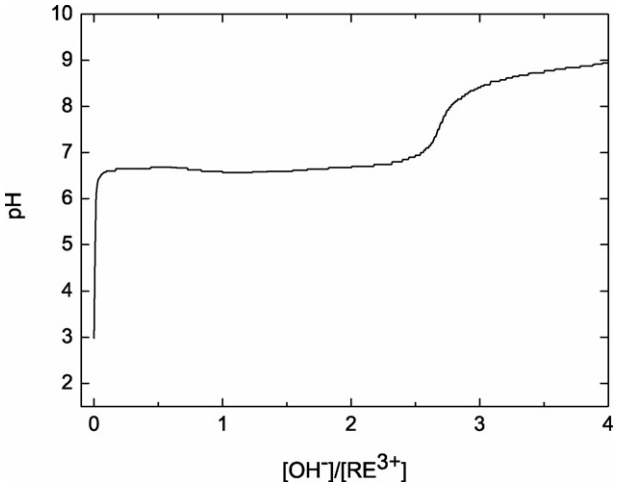

Fig. 8. pH curve of 2.7Yb:OH in function of reactant feed mole ratio.

equiaxed subunits of 100 nm or less. The size of these subunits is similar to the hydroxide particles obtained in gels precipitated at high supersaturation levels. Precipitation by ammonia water of all precursors occurred at a relatively constant pH of 7 (Fig. 8). However, supersaturation decreases all along when ammonia water is added into the nitrate solution, since yttrium, hydroxide and nitrate ions deplete, as they take part to the formation of the insoluble precipitate. Therefore, the chip-like particles are likely to have formed in the beginning of the precipitation run. Moreover, particles rich in ytterbium are also likely to precipitate in the beginning, since ytterbium becomes supersaturated first compared to yttrium when pH increases,[18] as shown in Fig. 9. Precipitation of the chip-like particles first is also consistent with the layer of platelets closely bonded to their surface. In fact, platelets can be thought as to have nucleated subsequently on the chip-like particles.

Chemical analysis results of trace elements obtained by ICP showed that both powders exhibit purities $\geq 99.9\%$. Both methods have therefore the ability to produce high purity powders.

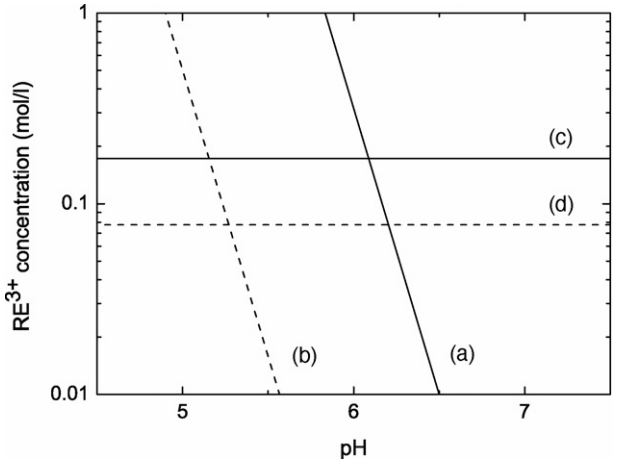

Fig. 9. Solubility of $Y(OH)_3$ (a) and $Yb(OH)_3$ (b) in function of pH. Nominal concentration of Y^{3+} (c) and Yb^{3+} (d). Solubility products were calculated from Ref.[18].

4. Conclusion

Precipitation of amorphous carbonate from yttrium and ytterbium nitrates enables to synthesise particles with uniform morphology and with an excellent distribution of ytterbium. This feature is attributed to the intimate mixing of the rare-earth cations in the amorphous particles as synthesised. This kind of synthesis can be therefore called a real co-precipitation.

However, in the investigated set of conditions, precipitation of yttrium and ytterbium nitrates by ammonia water leads to the formation of hydroxynitrate platelets, but also of ytterbium-rich particles with chip-like morphology. The chip-like particles are richer in ytterbium than the platelets, causing inhomogeneous distribution of ytterbium. Ytterbium gradients were still present after sintering in air at 1600 °C for 7 h.

The chip-like particles consist in dense agglomerates made of equiaxed hydroxide-based particles. The hard nature of these agglomerates prevents achieving good compaction densities during pressing, which leads to the formation of flaws during sintering.

Acknowledgements

The authors are grateful for the financial support from the Graduate School in Space Technology (Luleå, Sweden) and the Swedish Research Council.

References

[1]. Hönninger, C., Zhang, G., Keller, U. and Giesen, A., Femtosecond Yb-YAG laser using semiconductor saturable absorbers. *Opt. Lett.*, 1995, **20**, 2402.
[2]. van der Berg, R., Ytterbium challenges neodymium monopoly. *Opto Laser Eur.*, 2001(November).
[3]. Lu, J., Prabhu, M., Song, J., Li, C., Xu, J., Ueda, K. *et al.*, Optical properties and highly efficient laser oscillation of Nd:YAG ceramics. *Appl. Phys. B*, 2000, **71**, 469.
[4]. Lange, F. F., Sinterability of agglomerated powders. *J. Am. Ceram. Soc.*, 1984, **67**(2), 83–89.
[5]. Peelan, J. G. J., Influence of MgO on the evolution of the microstructure of Al_2O_3. *Mater. Sci. Res.*, 1975, **10**, 443–453.
[6]. Brenier, A., Boulon, G., Pedrini, C. and Madej, C., Effects of $Ca^{2+}Zr^{4+}$ ions pairs on spectroscopic properties of Cr^{3+}-doped $Gd_2Ga_5O_{12}$ garnets. *J. Appl. Phys.*, 1992, **71**(12), 6062–6068.
[7]. Ikegami, T., Li, J.-G. and Mori, T., Fabrication of transparent yttria ceramics by the low-temperature synthesis of yttrium hydroxide. *J. Am. Ceram. Soc.*, 2002, **85**(7), 1725–1729.
[8]. Saito, N., Matsuda, S.-I. and Ikegami, T., Fabrication of transparent yttria ceramics at low temperature using carbonate-derived powder. *J. Am. Ceram. Soc.*, 1998, **81**(8), 2023–2028.
[9]. Dupont, A., Parent, C., Le Garrec, B. and Heintz, J. M., Size and morphology control of Y_2O_3 nanopowders via a sol-gel route. *J. Solid State Chem.*, 2003, **171**, 152–160.
[10]. Li, J. G., Ikegami, T., Lee, J. H., Mori, T. and Yajima, Y., Co-precipitation synthesis and sintering of yttrium aluminium garnet (YAG) powders: the effect of precipitant. *J. Eur. Ceram. Soc.*, 2000, **20**, 2395–2405.
[11]. Li, J. G., Ikegami, T., Lee, J. H. and Mori, T., Well-sinterable $Y_2Al_5O_{12}$ powder from carbonate precursor. *J. Mater. Res.*, 2000, **15**(7), 1514–1523.
[12]. Li, J. G., Ikegami, T., Lee, J. H. and Mori, T., Characterization of yttrium aluminate garnet precursors synthesized via precipitation using ammonium bicarbonate as the precipitant. *J. Mater. Res.*, 2000, **15**(11), 2375–2386.

[13]. JCPDS cards no. 32–1435 and 49–1107.
[14]. Hachke, J. M., Preparation, phase equilibria, crystal chemistry, and some properties of lanthanide hydroxide nitrates. *Inorg. Chem.*, 1974, **13**(8).
[15]. JCPDS card no. 24–1419.
[16]. JCPDS card no. 41–1105.
[17]. Vegard, L., *Z. Kristallogr.*, 1928, **67**, 239.
[18]. Baes, C. F. and Mesmer, R. E., *The Hydrolysis of Cations*. John Wiley & Sons, Inc., New York, 1976.